Centered-rectangular lattice photonic-crystal surface-emitting lasers

Seita Iwahashi,[1,*] Kyosuke Sakai,[1,2] Yoshitaka Kurosaka,[1] and Susumu Noda[1,3]

[1]*Department of Electronic Science and Engineering, Kyoto University, Kyoto-Daigaku-Katsura, Nishikyo-ku, Kyoto 615-8510, Japan*

[2]*Pioneering Research Unit for Next Generation, Kyoto University, Goryo Ohara, 1-39, Nishikyo-ku, Kyoto 615-8245, Japan*

[3]*Photonics and Electronics Science and Engineering Center, Kyoto University, Kyoto-Daigaku-Katsura, Nishikyo-ku, Kyoto 615-8510, Japan*

(Received 8 June 2011; revised manuscript received 11 December 2011; published 6 January 2012)

We investigate the effects of lattice structure on the properties of photonic-crystal surface-emitting lasers. We analyze a general type of crystalline geometry known as the centered-rectangular lattice, which includes both square and triangular lattices. We theoretically and experimentally investigate the laser cavity characteristics of devices based on such photonic crystals, including the band structure and beam patterns, in order to explore the feasibility of two-dimensional (2D) lasing oscillation. The more general type of crystalline geometry represented by the centered-rectangular lattice should enable a comprehensive understanding of the 2D cavity characteristics to be achieved and also lead to further possibilities in the field of 2D photonic-crystal lasers.

DOI: 10.1103/PhysRevB.85.035304 PACS number(s): 42.55.Tv

I. INTRODUCTION

Two-dimensional (2D) photonic-crystal (PC) lasers, whose operation is based on the band-edge effect, provide spatially coherent beams over a broad area and for various wavelength ranges.[1–5] Coherent surface emission from the large cavity enables the construction of high-power single-mode lasers with various kinds of beam patterns.[6–8] The characteristics of a PC laser largely depend on the cavity design, i.e. the lattice-hole shape and lattice structure. The lattice-hole shape determines the output beam pattern; for example, circular holes produce a doughnut beam, and triangular holes produce a single-lobed beam.[6] Furthermore, the depth of the lattice holes greatly influences the output power.[9] The lattice structure determines the photonic band structure and hence the resonant mode properties at the band edges. It should be possible to utilize PCs with a range of 2D lattice types, but thus far only a few specific lattices have been analyzed.[1–14] Here, we examine a wider range of 2D PC lattice structures and analyze their cavity mode characteristics.

Most research involving 2D PCs has concentrated on triangular and square lattices [Figs. 1(a) and 1(b)], both of which are highly symmetric and give rise to a number of useful properties.[15,16] These two lattice structures are also typically utilized for 2D PC lasers. Both lattices fall within a more general type of 2D crystalline geometry, the centered-rectangular lattice. This lattice consists of two primitive translation vectors with the same size and arbitrary angles between them [Fig. 1(c)], which possesses a greater degree of structural flexibility. It is therefore interesting to study and obtain a comprehensive understanding of the basic characteristics of centered-rectangular 2D PCs as a function of structure, such as optical coupling phenomena, band structure, near- and far-field patterns, and the feasibility of achieving 2D lasing oscillation. Analysis of this expanded crystalline geometry might lead to cavities with novel properties and widen the possibilities of 2D PC lasers.

In this paper, we comprehensively investigate the cavity characteristics of centered-rectangular lattice PCs using both theory and experiment. In Sec. II, we describe the optical coupling phenomena in the reciprocal lattice space and calculate typical electromagnetic (EM) field distributions to demonstrate the presence of a 2D cavity mode. We analyze in detail cavity characteristics such as the photonic band structure and the diffraction process that gives rise to surface emission. In Sec. III, we describe the fabrication of devices with various centered-rectangular lattice structures and investigate their properties with an emphasis on beam patterns, spectra, and band structures. We then compare our experimental and theoretical results and discuss them in terms of 2D oscillation, lasing band-edge identification, and single-mode operation. Finally, concluding remarks are given in Sec. IV.

II. THEORETICAL ANALYSIS

Figure 2 shows a schematic picture of the PC laser structure, where the PC is used as a laser cavity. Previously, two typical types of lattice structures have been used in these devices, the square and triangular lattices shown in Figs. 1(a) and 1(b). The angle (ψ) between the two primitive translation vectors is 90° for the square lattice and 60° for the triangular lattice. Figure 1(c) shows the centered-rectangular lattice, in which ψ can vary from 0° to 90° (the dotted line indicates a centered rectangle). Therefore, by adopting ψ as a variable parameter, we can investigate the potential of a much wider range of lattice structures than the square and triangular lattices alone. We used the plane wave expansion method to obtain the EM field distributions and band structures described below. The dielectric constants of the air holes (ε_a) and the background (ε_b) were assumed to be 10.3 and 11.8, respectively, following Ref. 17.

A. Fundamental modes in centered-rectangular lattice structure

Figures 3(a)–3(c) show the reciprocal lattice space corresponding to the real space in Fig. 1. The arrows represent fundamental wave vectors, which have the same wave number at the Γ points. Four equivalent wave vectors exist for the square lattice [Fig. 3(a)] and six for the triangular lattice [Fig. 3(b)]. These wave vectors couple with each other and produce cavity modes.[11,12] In a similar way, the centered-rectangular lattice possesses four equivalent fundamental wave vectors that couple with each other. These four vectors form a 2D plane; therefore, the cavity modes should also be distributed in the same plane.[18]

 ©2012 American Physical Society

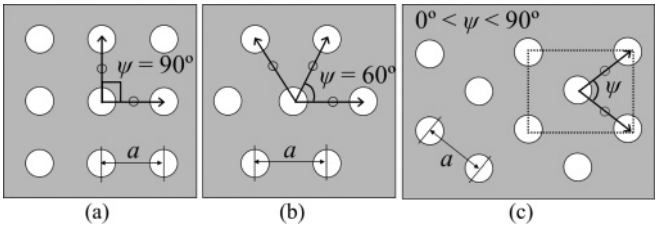

FIG. 1. Lattice structures of two-dimensional photonic crystals: (a) square lattice, (b) triangular lattice, and (c) centered-rectangular lattice. The angle (ψ) between the primitive translation vectors is 90° for the square lattice and 60° for the triangular lattice.

We calculated typical EM field distributions in the PC plane to confirm the formation of two-dimensionally oscillating modes, for which the field distribution has a two-dimensional periodicity (both in the x and y directions), because one-dimensionally oscillating modes, for which the field distribution has a periodicity only in a specific direction, may be formed even in 2D lattice.[2,11] Figures 4(a)–4(d) show the EM field distribution for four fundamental modes in the case of $\psi = 50°$, arranged from the lowest frequency mode (a) to the highest frequency mode (d). The four corresponding band edges are indicated by the black arrow in Fig. 5(e). It is clear that all four modes are 2D mode, which was also confirmed for various other values of ψ. From this result, we can conclude that the centered-rectangular lattice structure is suitable for operation as a 2D PC laser.

B. Photonic band structure

In this section, we investigate the band structure, the number of band-edge cavity modes, and their frequency gap widths as a function of ψ. Figures 5(a)–5(f) show the band structures of PCs with ψ varying from 90° to 40° in steps of 10°. The enlarged band structure diagrams in the insets show the fundamental cavity modes at the Γ point, indicated by the black arrows, which are produced by the fundamental wave vectors in Fig. 3.

The number of fundamental cavity modes depends on the lattice structure. In the range of ψ considered here, six modes are found only for $\psi = 60°$ and four for all other values of ψ. This observation can be schematically understood by focusing on the two modes indicated by the blue circle in each diagram, which move to lower frequency as ψ decreases. When $\psi = 60°$, these modes almost coincide with the other four fundamental cavity modes, increasing the mode number

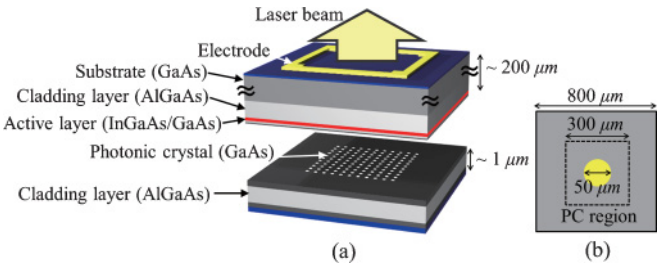

FIG. 2. (Color online) Schematic pictures of (a) a photonic crystal laser structure and (b) the bottom side of the device. The laser beam is emitted from the surface of the device.

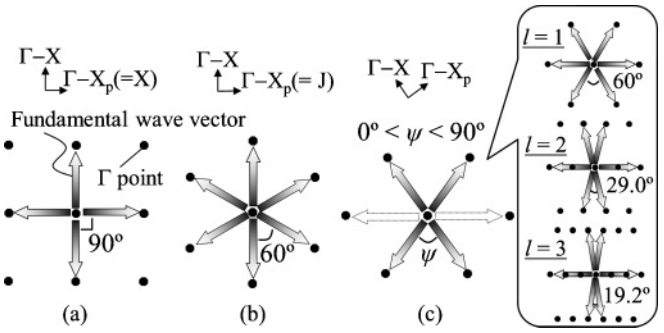

FIG. 3. Reciprocal lattice space corresponding to the real space in Fig. 1. Two-dimensional cavity modes are formed by the coupling of (a) four equivalent wave vectors for the square lattice, (b) six for the triangular lattice, and (c) four for the centered-rectangular lattice. The inset shows the special cases of centered-rectangular lattice, where the number of equivalent wave vectors becomes six according to Eq. (1).

to six. The mode number corresponds to the number of fundamental waves, which is six for the triangular lattice [Fig. 3(b)] and four for the square lattice [Fig. 3(a)]. In the case of the centered-rectangular lattice in Fig. 3(c), the number of fundamental waves is generally four but increases to six when the wave number of the two Γ points in the horizontal direction (indicated by the dotted arrow) matches that of the other four Γ points. Analytically, the number of fundamental waves becomes six when ψ satisfies the following condition:

$$\psi = 2\sin^{-1}\left(\frac{1}{2l}\right), \tag{1}$$

where l is an integer, which is the order of the Γ points in the horizontal direction. Accordingly, the mode number becomes six when $\psi = 60.0°$ ($l = 1$), 29.0° ($l = 2$), 19.2° ($l = 3$),. . ., of which the fundamental wave distribution are shown in the inset of Fig. 3(c). In these conditions, two waves in the horizontal direction interfere with the original four waves; therefore, six cavity modes are produced, and their properties specifically differ from the original four modes.[19]

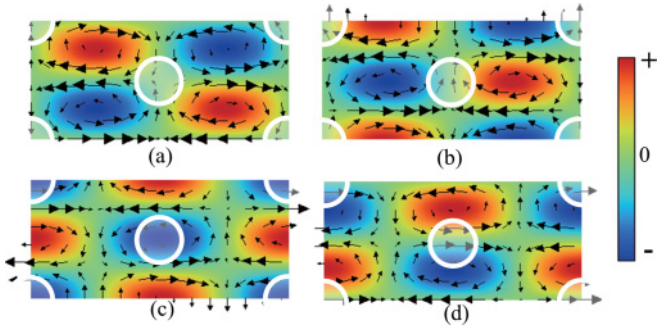

FIG. 4. (Color online) Electromagnetic field distributions in the PC plane for four fundamental modes, (a) the lowest frequency mode to (d) the highest frequency mode, in the centered-rectangular lattice with $\psi = 50°$. The white circles are lattice holes. Shading represents the magnetic field intensity, and arrows represent the electric field vectors. The electromagnetic field is distributed in two dimensions.

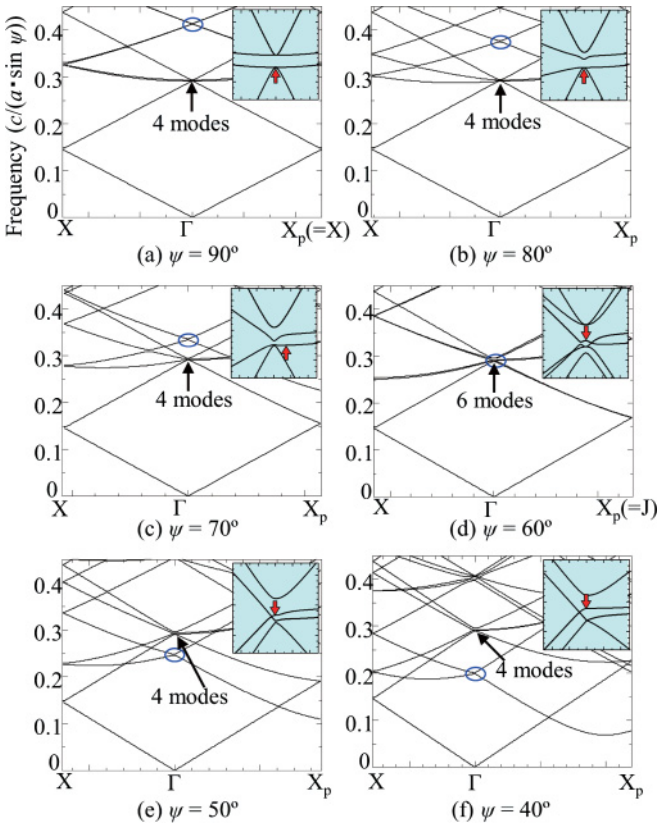

FIG. 5. (Color online) Band structures of centered-rectangular lattice PCs with ψ ranging from (a) 90° to (f) 40° in steps of 10°. The left-hand side of the plots shows the Γ-X axis, and the right-hand side shows the Γ-X_p axis (perpendicular to Γ-X). The fundamental cavity modes at the Γ point are indicated by the black arrow in each case and shown in greater detail in the insets. The blue/medium gray circle in each plot indicates two modes that move to lower frequency as ψ decreases and coincide with the other four Γ-point modes at $\psi = 60°$. Red/dark gray arrows indicate the lasing band edges.

The band-edge frequencies and their corresponding gap widths at the Γ points are also closely dependent on the lattice structure. The band-edge frequencies ($\omega_{A,B,C,D}$) of the four fundamental modes can be analytically expressed as follows, according to coupled wave theory (see Appendix):

$$\begin{aligned}\omega_A &= c/n[\beta_0 - \kappa_3 - \cos\psi(\kappa_{2a} - \kappa_{2b})]\\ \omega_B &= c/n[\beta_0 - \kappa_3 + \cos\psi(\kappa_{2a} - \kappa_{2b})]\\ \omega_C &= c/n[\beta_0 + \kappa_3 - \cos\psi(\kappa_{2a} + \kappa_{2b})]\\ \omega_D &= c/n[\beta_0 + \kappa_3 + \cos\psi(\kappa_{2a} + \kappa_{2b})].\end{aligned} \tag{2}$$

Here, n is the refractive index, and c is the speed of light in vacuum. The parameters κ_{2a}, κ_{2b}, and κ_3 are coupling constants defined in Eqs. (A4)–(A6). Figure 6 shows a schematic plot of the band-edge frequencies and gaps, as well as the Bragg frequency β_0, where c/n is normalized as 1. The gap width between two band edges is determined by the coupling constant and lattice angle ψ, where ψ is a particularly significant parameter because cos ψ varies from 0 to 1. The gap widths also strongly depend on the strengths of the respective light wave couplings. The constant κ_3 represents the coupling of waves in opposite directions, as shown in Fig. 7(a). This is

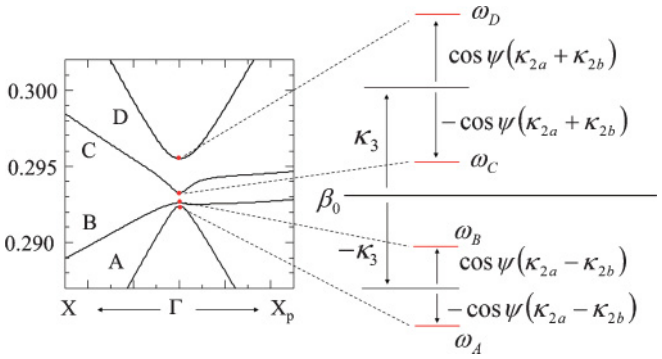

FIG. 6. (Color online) Gap widths for band-edge frequencies ω_A-ω_D. The gap widths depend on the coupling constants κ and the lattice angle ψ.

the same as the backward scattering in second-order distributed feedback lasers. The constants κ_{2a} and κ_{2b} represent the 2D coupling of waves that are at oblique angles to each other [Figs. 7(b) and 7(c)]. Therefore, the gaps between ω_A and ω_B and between ω_C and ω_D are related to the 2D coupling strength, whereas the gap between the center of ω_A and ω_B and the center of ω_C and ω_D is related to the backward coupling strength.

In this manner, the lattice structure strongly influences both the entire and local band structure, including the mode number and the band gap. Tuning the lattice structure may thus enable more flexible control of the band structure and allow the restriction of unwanted band edges or the generation of new band edges.[24,25]

In this coupled wave model for the centered-rectangular lattice, we have performed our analysis using four fundamental waves. However, a more advanced coupled-wave model should be used if appropriate. For example, in the case of $\psi = 90°$, at least eight waves should be considered in order to express the 2D coupling.[11] In the four-wave model, cos ψ is 0, and 2D coupling cannot be expressed. Furthermore, in the case of $\psi = 60°$, the number of fundamental waves is six by symmetry. Therefore, at least six waves are needed to formulate the basic coupling model.[12]

C. Radiation effect

We now describe the diffraction process that gives rise to surface emission, and we study the dependence of the output beam directions on ψ. A fundamental wave at a Γ point is coupled to waves at the other Γ points by the diffraction effect of the PC.[9] If one or more Γ points is inside the light cone, then

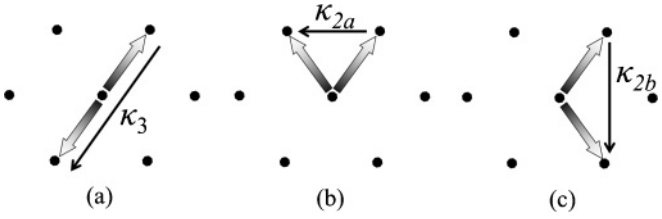

FIG. 7. Diffraction diagrams for coupling constants of (a) κ_3, (b) κ_{2a}, and (c) κ_{2b}. Shaded arrows indicate pairs of wave vectors, and black arrows indicate the corresponding reciprocal lattice vectors.

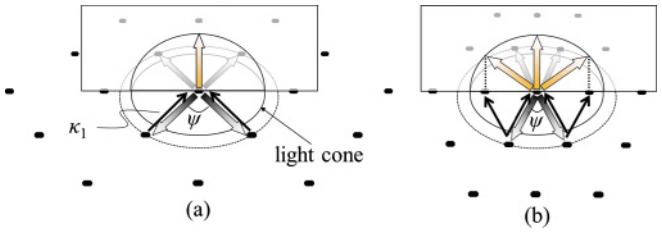

FIG. 8. (Color online) Schematic picture of radiation processes for two representative cases. The fundamental waves are diffracted via coupling constant κ_1. (a) There is only one Γ point inside the light cone, at the center, and the output beam is radiated in the normal direction. (b) There are three Γ points inside the light cone, one at the center and two at either side. The output beam is radiated in three different directions.

surface emission occurs. The directions of the output beams are determined by the in-plane wave numbers of the Γ points in the light cone, which can be controlled by the angle ψ.

For example, in Fig. 8(a), there is only one Γ point inside the light cone, at the center, and the in-plane wave number is zero. In this case, by the diffraction of κ_1 [Fig. 16] to the central Γ point, the output beam propagates in the normal direction. In the case of Fig. 8(b), where ψ is much smaller than in Fig. 8(a), there are Γ points both at the center of the light cone and within the cone on the right- and left-hand sides. The output beams propagate in three directions: the vertical direction (0th order) and at an oblique angle to the left and right (±1st order). The ±1st-order beams are emitted when the condition $\psi < 2\sin^{-1}(1/2r_n)$ is satisfied; the direction can be varied with ψ. The beam angle (θ), as referred to the normal direction, is expressed as

$$\theta_{\pm 1} = \pm \sin^{-1}\left[2r_n \cdot \sin(\psi/2)\right], \tag{3}$$

where $r_n = n_{\mathrm{eff}}/n_{\mathrm{clad}}$. n_{eff} is the effective refractive index in the core, including the active and PC layers, and n_{clad} is the refractive index of the cladding layers. As ψ is decreased further, the number of Γ points in the light cone increases, adding ±2nd- and ±3rd-order beams. The mth-order beam angle (θ_m) can be expressed as

$$\theta_m = \sin^{-1}\left[2r_n m \sin(\psi/2)\right], \qquad [\psi < 2\sin^{-1}(1/2r_n m)]. \tag{4}$$

In this manner, ψ determines the directions of the output beams.

III. EXPERIMENTAL RESULTS

We next fabricated devices with various lattice structures and evaluated properties such as their far- and near-field patterns, spectra, and photonic band structures. As shown in Fig. 2(a), the PC and active layers are sandwiched by cladding layers for the confinement of both light and carriers. This structure was fabricated using the wafer-fusion technique after the PCs, as a laser cavity, were made in the 300-μm square field.[23] The current is injected from the bottom side through a circular electrode with a 50-μm diameter shown in Fig. 2(b), which is 1 μm away from the PC layer and restricts the area of current flow. We designed six kinds of lattice structures in

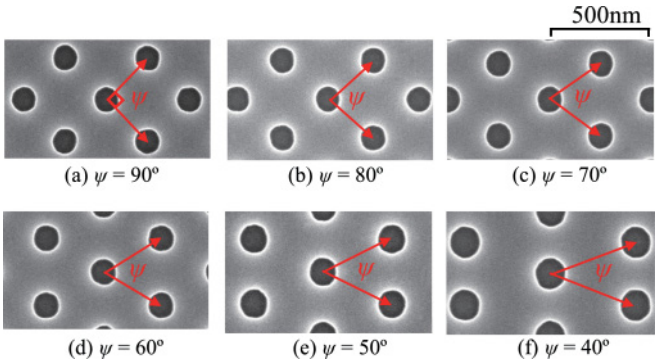

FIG. 9. (Color online) Scanning electron microscope (SEM) images of six fabricated PCs with ψ ranging from (a) 90° to (f) 40° in steps of 10°.

which ψ ranged from 90° to 40° in steps of 10°. The scanning electron microscope (SEM) images of the devices are shown in Figs. 9(a)–9(f). The lattice holes were circular in shape, and the filling factor was fixed at 12%, except for the $\psi = 60°$ structure, where it was 9%. When we injected a pulsed current (1 kHz, 500 ns), we successfully obtained lasing for all the lattice types. A near-field pattern and its spectra, showing Γ-point oscillation for a typical device with $\psi = 80°$, is presented in Fig. 10. Single-mode lasing was observed throughout the 2D plane. This represents the first demonstration of 2D single-mode oscillation from 2D PC lasers with the centered-rectangular lattice structure. Figure 11 shows the far-field patterns for our devices. In all cases except the $\psi = 70°$ structure, a doughnut beam or two-lobed beam radiating in the normal direction (Γ-point oscillation) was obtained. In contrast, the device with $\psi = 70°$ emitted twin beams tilted at an angle of 4° (non-Γ-point oscillation).

First, we will examine the case of Γ-point oscillation, which was obtained from all the devices except for the $\psi = 70°$ structure. Although the devices with $\psi = 50°$ and 40° produce oblique ±1st-order beams according to Eq. (3), they are not emitted from the device due to total internal reflection at the

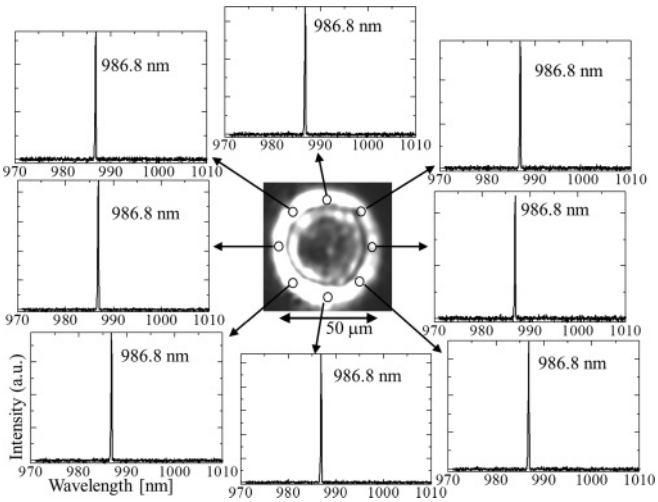

FIG. 10. A near-field pattern and its spectra for a typical fabricated device with $\psi = 80°$, demonstrating Γ-point lasing. A single-mode oscillation was observed throughout the 2D plane.

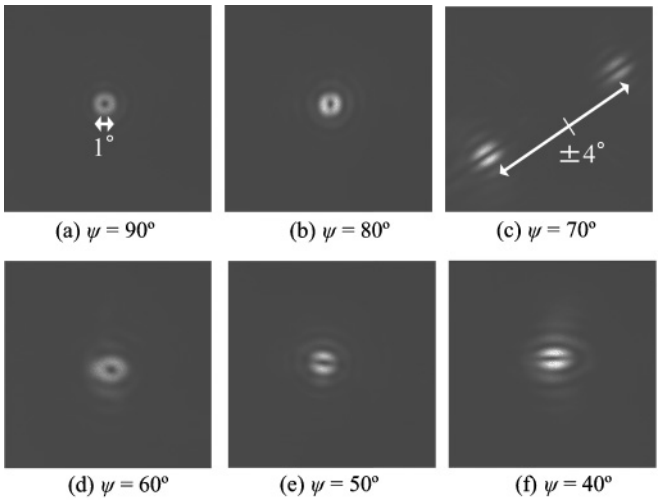

FIG. 11. Far-field patterns for our fabricated devices with centered-rectangular lattice PCs with ψ ranging from (a) 90° to (f) 40° in steps of 10°. The device with (c) $\psi = 70°$ emitted twin beams tilted at 4°, corresponding to a non-Γ-point mode; all the other devices emitted a doughnut beam or two-lobed beam in the vertical direction. The beam divergence angle is ∼1°, indicating 2D large-area oscillation in the PC plane.

surface of the GaAs substrate (air-semiconductor interface above the cladding). Therefore, an output beam is obtained only in the vertical direction for all the devices discussed here. The beam divergence angle is ∼1°, which indicates large-area oscillation in the PC plane. The oscillated mode can be identified from among several band edges by angle-resolved electroluminescence subthreshold measurement.[17] Figure 12(a) shows the measured band structure of the centered-rectangular lattice with $\psi = 50°$, together with the lasing spectrum. Figure 12(b) shows the corresponding calculated band structure. By comparing Figs. 12(a) and 12(b), we can determine that the laser oscillation occurs at the third band edge from the bottom, indicated by an arrow. Furthermore, the correspondence of the beam pattern to the EM field distribution in the PC plane supports the assignment of laser oscillation to this band edge. Figure 13(a) shows the beam pattern and its polarization for the $\psi = 50°$ structure, and Fig. 13(b) shows the EM field distribution over one unit cell inside the PC layer. The beam patterns is basically determined by the symmetry of the mode at the symmetry point when the

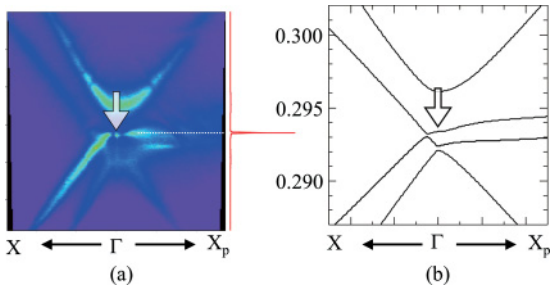

FIG. 12. (Color online) (a) Measured and (b) calculated band structure of the PC with $\psi = 50°$. The lasing spectrum is shown on the right-hand side of (a) by a red/dark gray curve. The lasing band edge is indicated by the arrow.

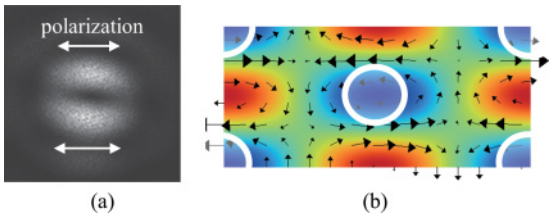

FIG. 13. (Color online) (a) Beam pattern and its polarization for the fabricated device with $\psi = 50°$. (b) Calculated EM field distribution of the third band-edge mode over one unit cell inside the PC layer. Because the electric-field component in the horizontal direction is dominant, the polarization of the two-lobed far-field pattern is also horizontal.

envelop of the cavity mode is a Gaussian-like (single-lobe) spacial distribution, excited from the center part of the PC region away from the boundary, which also correspond to the lowest longitudinal mode requiring the smallest threshold gain.[11] The electric field components are antisymmetric with respect to the center of the lattice hole. When the light is diffracted normal to the PC plane, the antisymmetric nature of the electric field causes destructive interference, giving rise to zero intensity at the center of the output beam. This is a similar scenario to the azimuthally polarized doughnut beams described in Refs. 24 and 25, although in the present case, the horizontal component is dominant. Similar considerations allowed the lasing band edges of our other devices to be identified; the relevant modes are indicated by red arrows in Fig. 5. Figures 14(a)–14(e) show the corresponding EM field distributions. These lasing modes appear to have the same origin, giving rise to similar symmetric field distributions, where magnetic field antinodes are located in the centers of the lattice holes, and the electric field components rotate around the lattice holes.

In this paper, although we have not calculated the radiation loss of centered-rectangular lattice cavities, we can discuss the mode selection among Γ-point modes by referring to Ref. 11, the case of the square lattice. First, the vertical radiation loss plays a key role for determining the selection of the lasing

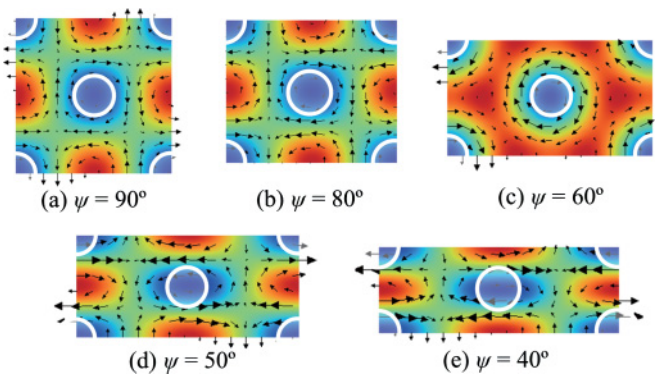

FIG. 14. (Color online) EM field distributions in the PC plane corresponding to the modes indicated by red/dark gray arrows in Fig. 5 with ψ = (a) 90°, (b) 80°, (c) 60°, (d) 50°, and (e) 40°. The symmetry of these distributions is similar for all modes, with magnetic field antinodes at the centers of the lattice holes and electric field components rotating around the lattice holes.

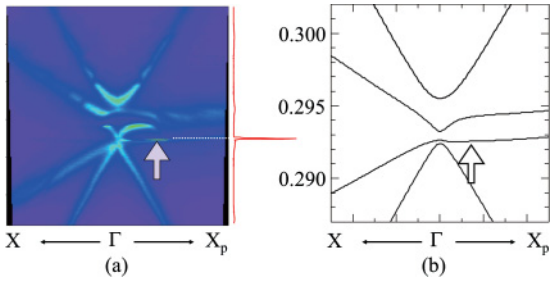

FIG. 15. (Color online) (a) Measured and (b) calculated band structures for the non-Γ-point oscillation in the $\psi = 70^\circ$ structure. The oscillated mode is at the non-Γ-point on the Γ-X_p axis (flat band) indicated by the arrow.

band edge. In Fig. 4, the electric field of the modes (a) and (c) are antisymmetric, causing the destructive interference in the vertical direction. This means that the radiation from these modes should be inefficient (dark mode), and the vertical loss is suppressed compared with the other two modes (b) and (d). Therefore, we can predict the mode (a) or (c) will contribute the lasing in terms of the modal symmetry. Secondly, the in-plane radiation loss has an influence on the mode selection among those two dark modes. For the case of square lattice, the EM field distribution, similar to that shown in Fig. 4(c), provides lower radiation loss than the mode with the EM field distribution, as in Fig. 4(a), because the difference of the envelope of the considered modes produces the difference of the in-plane radiation loss. In fact, all the devices with Γ-point oscillation in this paper can be estimated to be lased with the EM field distribution shown in Fig. 14, and these EM fields possess the same symmetry with the modes shown in Fig. 4(c).

Finally, we examine the non-Γ-point oscillation arising in the device with $\psi = 70^\circ$. In a similar way to Fig. 12, the lasing mode was determined to be the mode at the non-Γ-point on the Γ-X_p axis indicated by the arrow in Fig. 15(a). There is always a slow-group-velocity band (flat band) on the Γ-X_p axis, as shown in Fig. 5; and a band edge, which is a zero-group-velocity point, is often found on this flat band, as shown in Fig. 15(b).[20,22] As a result of the higher Q factor at the band edge on the flat band compared to the other Γ-point band edges, non-Γ-point oscillation occurs in this case. We note that a flat band on the Γ-X_p axis also exists in the band structure of the $\psi = 50^\circ$ device in Fig. 12(b), but not with a band edge. This may suggest that varying ψ also allows the flat band characteristics to be altered, which would enable Γ-point or non-Γ-point oscillation to be selected.

IV. CONCLUSION

We have comprehensively investigated the cavity characteristics of PC lasers based on the centered-rectangular lattice structure, which spans a general class of lattice structures that includes the conventionally analyzed square and triangular lattices. We have theoretically confirmed the presence of a 2D cavity mode in the centered-rectangular lattice by considering the optical coupling phenomena and calculating the EM field distributions. We have closely analyzed cavity characteristics such as the photonic band structure and the diffraction process that gives rise to surface emission. These characteristics are strongly influenced by the lattice structure, allowing control of the number of band edges and their gaps, as well as the directions of the output beams.

We have also evaluated the properties of fabricated devices with different centered-rectangular lattice structures, with emphasis on the far- and near-field patterns, spectra, and band structures. Two kinds of lasing were obtained, resulting from Γ-point and non-Γ-point oscillation and were compared with theoretically obtained band structures and polarizations for the same lattice structures. We have demonstrated that 2D, single-mode lasing oscillation can be obtained from most devices with the centered-rectangular lattice. The expansion in available structural degrees of freedom provided by the centered-rectangular lattice, as well as the comprehensive understanding of cavity characteristics as a function of structure provided by our study, will lead to further possibilities in the field of 2D PC lasers.

ACKNOWLEDGMENTS

The authors are grateful to K. Ishizaki, C. Peng, and Y. Liang for valuable suggestions. This work was partly supported by Core Research for Evolution Science and Technology of the Japan Science and Technology Agency (CREST-JST) and by the Global COE Program. S. Iwahashi is supported by the Research Fellowship of the Japan Society for Promotion of Science.

APPENDIX: DEVIATIONS OF BAND EDGE FREQUENCY IN CENTERED-RECTANGULAR LATTICE PHOTONIC CRYSTAL WITH TE POLARIZATION

Below we use coupled mode theory to derive the equation for the band-edge frequency at the Γ point for the centered-rectangular lattice. The basic derivation is given in Ref. 11. Here, we only show the parts of the derivation that have been modified, such as the definition of the fundamental lattice vectors and the coupling model.

Two fundamental lattice vectors $\mathbf{a}_1$ and $\mathbf{a}_2$ in a centered-rectangular lattice can be written as

$$\begin{aligned} \mathbf{a}_1 &= [a\cos(\psi/2), -a\sin(\psi/2)] \\ \mathbf{a}_2 &= [a\cos(\psi/2), a\sin(\psi/2)] \end{aligned} \tag{A1}$$

where a is the lattice constant, and ψ is the angle between the fundamental lattice vectors. The fundamental reciprocal lattice vectors $\mathbf{b}_1$ and $\mathbf{b}_2$ are written as

$$\begin{aligned} \mathbf{b}_1 &= [\beta_0\sin(\psi/2), -\beta_0\cos(\psi/2)] \\ \mathbf{b}_2 &= [\beta_0\sin(\psi/2), \beta_0\cos(\psi/2)] \end{aligned} \tag{A2}$$

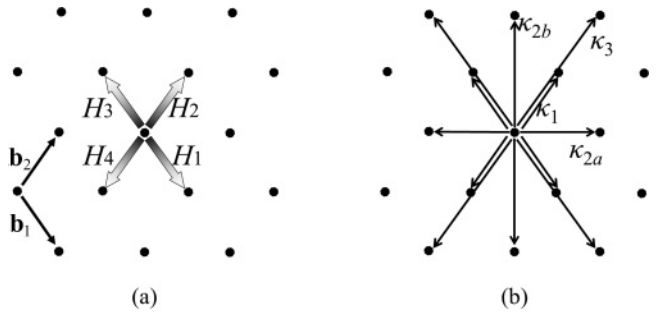

FIG. 16. Definition of (a) fundamental wave vectors and (b) coupling constants considered in this paper.

where $\beta_0 = 2\pi/(a \sin\psi)$.

We consider the z component of the magnetic field (H_z) as a basic wave vector for transverse electric (TE) polarization. The fundamental wave vectors are shown in Fig. 16, and we define H_z as

$$\begin{aligned} H_z(\mathbf{r}) &= H_1 e^{-i\beta_0[\sin(\psi/2)x - \cos(\psi/2)y]} + H_2 e^{i\beta_0[\sin(\psi/2)x + \cos(\psi/2)y]} \\ &\quad + H_3 e^{i\beta_0[\sin(\psi/2)x - \cos(\psi/2)y]} + H_4 e^{-i\beta_0[\sin(\psi/2)x + \cos(\psi/2)y]} \end{aligned} \tag{A3}$$

where H_i are the magnitudes of the respective fundamental waves.

We also define the coupling constants that express the coupling of the wave vectors. The coupling constants for $|\mathbf{G}| = 2\beta_0 \cdot \sin(\psi/2)$, $2\beta_0 \cdot \cos(\psi/2)$, and $2\beta_0$ contribute significantly. These coupling constants are shown in Fig. 16, and we list them as:

$$\kappa_{2a} \equiv \kappa_{\mathbf{G}(\pm1,\pm1)} = \kappa_{\mathbf{G}}|_{|\mathbf{G}|=2\beta_0 \sin(\psi/2)}, \tag{A4}$$

$$\kappa_{2b} \equiv \kappa_{\mathbf{G}(\pm1,\mp1)} = \kappa_{\mathbf{G}}|_{|\mathbf{G}|=2\beta_0 \cos(\psi/2)}, \tag{A5}$$

$$\kappa_3 \equiv \kappa_{\mathbf{G}(\pm2,0)} = \kappa_{\mathbf{G}(0,\pm2)} = \kappa_{\mathbf{G}}|_{|\mathbf{G}|=2\beta_0 \sin(\psi/2)}, \tag{A6}$$

where $\kappa_{\mathbf{G}}$ is defined as,[11,12]

$$\kappa_{\mathbf{G}} = -\frac{\pi}{\lambda \varepsilon_0^{1/2}} \varepsilon_{\mathbf{G}}, \tag{A7}$$

where $\varepsilon_{\mathbf{G}}$ is the Fourier coefficient of the modulated dielectric constant $\varepsilon(\mathbf{r})$. The coupling constants can be real numbers because we assume a symmetric structure such as that given by circular lattice holes.

Using Eqs. (A4)–(A6) and solving Maxwell's equations [Eqs. (5)–(9) in Ref. 11, we obtain four equations of the form:

$$\begin{aligned} \delta H_1 &= \kappa_3 H_3 - \cos\psi\kappa_{2a} H_4 + \cos\psi\kappa_{2b} H_2 \\ \delta H_2 &= \kappa_3 H_4 - \cos\psi\kappa_{2a} H_3 + \cos\psi\kappa_{2b} H_1 \\ \delta H_3 &= \kappa_3 H_1 - \cos\psi\kappa_{2a} H_2 + \cos\psi\kappa_{2b} H_4 \\ \delta H_4 &= \kappa_3 H_2 - \cos\psi\kappa_{2a} H_1 + \cos\psi\kappa_{2b} H_3 \end{aligned} \tag{A8}$$

where δ is the deviation from the Bragg condition.

The above set of equations expresses the coupling of waves propagating in the centered-rectangular lattice PC structure. For example, the first expression in Eq. (A8) describes the coupling of waves H_1 and H_3 that travel in opposite directions; the intensity of the coupling is given by κ_3. The same equation also describes the coupling of waves that propagate at an oblique angle to each other. That is, wave H_1 couples to waves H_4 and H_2 with an intensity of $\cos\psi\kappa_{2a}$ and $\cos\psi\kappa_{2b}$, respectively. These oblique couplings provide 2D optical feedback, which gives rise to coherent 2D oscillation.

Solving Eq. (A8) as an eigenequation, the eigenvalue δ is given as

$$\delta = \begin{cases} \kappa_3 + \cos\psi(\kappa_{2a} + \kappa_{2b}) \\ \kappa_3 - \cos\psi(\kappa_{2a} + \kappa_{2b}) \\ -\kappa_3 + \cos\psi(\kappa_{2a} - \kappa_{2b}) \\ -\kappa_3 - \cos\psi(\kappa_{2a} - \kappa_{2b}) \end{cases}. \tag{A9}$$

From Eq. (A9) and the relation $\omega = (c/n)\beta = (c/n)(\delta + \beta_0)$, the expression for the band-edge frequencies in Eq. (2) is derived.

*Corresponding author: Dr. Seita Iwahashi, Department of Electronic Science and Engineering, Kyoto University, Noda lab. A1-328 Kyoto Daigaku, Katsura Nishikyo-ku Kyoto-shi, Japan; iwahashi@qoe.kuee.kyoto-u.ac.jp

[1] M. Imada, S. Noda, A. Chutinan, T. Tokuda, M. Murata, and G. Sasaki, Appl. Phys. Lett. **75**, 316 (1999).
[2] S. Noda, M. Yokoyama, M. Imada, A. Chutinan, and M. Mochizuki, Science **293**, 1123 (2001).
[3] R. Colombelli, K. Srinivasan, M. Troccoli, O. Painter, C. F. Gmachl, D. M. Tennant, A. M. Sergent, D. L. Sivco, A. Y. Cho, and F. Capasso, Science **302**, 1374 (2003).
[4] H. Matsubara, S. Yoshimoto, H. Saito, Y. Jianglin, Y. Tanaka, and S. Noda, Science **319**, 445 (2008).
[5] L. Sirigu, R. Terazzi, M. Amanti, M. Giovannini, and J. Faist, Opt. Express **16**, 5206 (2008).
[6] E. Miyai, K. Sakai, T. Okano, W. Kunishi, D. Ohnishi, and S. Noda, Nature **441**, 946 (2006).
[7] E. Miyai, K. Sakai, T. Okano, W. Kunishi, D. Ohnishi, and S. Noda, Appl. Phys. Exp. **1**, 062002 (2008).
[8] S. Iwahashi, Y. Kurosaka, K. Sakai, K. Kitamura, N. Takayama, and S. Noda, Opt. Express **19**, 11963 (2011).
[9] S. Iwahashi, K. Sakai, K. Yoshitaka, and S. Noda, J. Opt. Soc. Am. B **27**, 1204 (2010).
[10] I. Vurgaftman and J. R. Meyer, Appl. Phys. Lett. **78**, 1475 (1999).
[11] K. Sakai, E. Miyai, and S. Noda, IEEE J. Quantum Elect. **46**, 788 (2010).
[12] K. Sakai, J. Yue, and S. Noda, Opt. Express **16**, 6033 (2008).
[13] A. R. Alija, L. J. Martinez, P. A. Postigo, J. Sanchez-Dehesa, M. Galli, A. Politi, M. Patrini, L. C. Andreani, C. Seassal, and P. Viktorovitch, Opt. Express **15**, 704 (2007).
[14] A. V. Giannopoulos, C. M. Long, and K. D. Choquette, Electron. Lett. **44**, 13 (2008).
[15] Y. Akahane, T. Asano, B. S. Song, and S. Noda, Nature **425**, 944 (2003).

[16]H. Y. Ryu, S. H. Kim, H. G. Park, J. K. Hwang, Y. H. Lee, and J. S. Kim, Appl. Phys. Lett. **80**, 3883 (2002).
[17]K. Sakai, E. Miyai, T. Sakaguchi, D. Ohnishi, T. Okano, and S. Noda, IEEE J. Sel. Areas Commun. **23**, 1335 (2005).
[18]M. Notomi, H. Suzuki, and T. Tamamura, Appl. Phys. Lett. **78**, 1325 (2001).
[19]M. Imada, A. Chutinan, S. Noda, and M. Mochizuki, Phys. Rev. B **65**, 195306 (2002).
[20]K. Forberich, M. Diem, J. Crewett, U. Lemmer, A. Gombert, and K. Busch, Appl. Phys. B **82**, 539 (2006).
[21]Y. Kurosaka, S. Iwahashi, K. Sakai, E. Miyai, W. Kunishi, D. Ohnishi, and S. Noda, IEICE Electron. Express **6**, 966 (2009).
[22]Y. Kurosaka, S. Iwahashi, Y. Liang, K. Sakai, E. Miyai, W. Kunishi, D. Ohnishi, and S. Noda, Nature Photon. **4**, 447 (2010).
[23]D. Ohnishi, T. Okano, M. Imada, and S. Noda, Opt. Express **12**, 1562 (2004).
[24]G. A. Turnbull, P. Andrew, W. L. Barnes, and I. D. Samuel, Appl. Phys. Lett. **82**, 313 (2003).
[25]K. Sakai and S. Noda, Electron. Lett. **43**, 107 (2007).